ACS APPLIED MATERIALS & INTERFACES

Research Article

www.acsami.org

# Bio-based Ionic Liquid Crystalline Quaternary Ammonium Salts: Properties and Applications

Renjith Sasi, Talasila P. Rao, and Sudha J. Devaki*

Chemical Sciences and Technology Division, CSIR-National Institute for Interdisciplinary Science and Technology (CSIR-NIIST), Thiruvananthapuram, 695019, India

Supporting Information

**ABSTRACT:** In the present work, we describe the preparation, properties, and applications of novel ionic liquid crystalline quaternary ammonium salts (QSs) of 3-pentadecylphenol, a bio-based low-cost material derived from cashew nut shell liquid. Amphotropic liquid crystalline phase formation in QSs was characterized using a combination of techniques, such as DSC, PLM, XRD, SEM, and rheology, which revealed the formation of one, two, and three dimensionally ordered mesophases in different length scales. On the basis of these results, a plausible mechanism for the formation of specific modes of packing in various mesophases was proposed. Observation of anisotropic ionic conductivity and electrochemical stability suggests their application as a solid electrolyte.

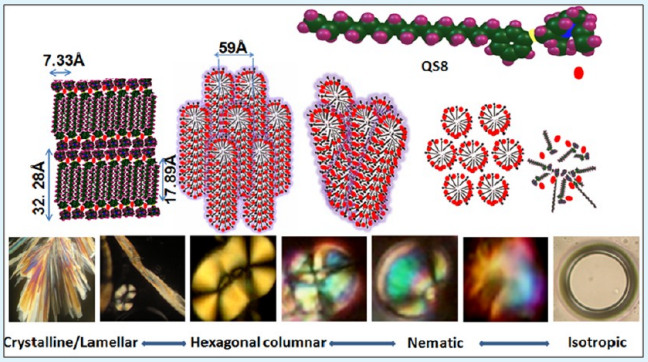


**KEYWORDS:** *ionic liquid crystals, self-assembly, soft template, rheology, hexagonal columnar, conducting gels*

## INTRODUCTION

Ionic liquid crystals (ILCs) are unique molecules having combined properties of liquid crystals (LCs) and ionic liquids (ILs). They find applications in areas such as energy storage devices, sensors, regioselective synthesis, anisotropic conductors, separation membranes, power sources, and so forth.[1−4] ILCs form mesophases through various noncovalent interactions and may exhibit properties such as macroscopic orientation, ionic conductivity, and the transportation of charges in liquid crystalline phases. The nature of mesogenic phases in ILCs is governed by the molecular shape, dimensions of the molecules and location of the ionic parts in the molecules, molecular interactions, and microphase segregation.[5] Among the various types of ILCs, imidazolium- or pyridinium-based salts containing weakly coordinating anions, such as $BF_4^-$ and $PF_6^-$, are well-known because of their high thermal and electrochemical stabilities.[6,7] However, quaternary ammonium salts (QAS) are receiving importance in widespread industrial utilization due to their high surface activity, less aqueous toxicity, and resistance to oxidation and reduction process.[8] Research on the development of QAS-based ionogels with a wider electrochemical window is also receiving importance for their application as electrolytes in solid ion batteries and supercapacitors due to the anisotropic conduction mechanism.[9−12]

Because of the overwhelming interest in the applications of ILCs and also because of the rapid depletion of petroleum-based products, researchers are in search of alternative cheaper, easily and abundantly available renewable resource based molecules. Cardanol (3-pentadecylphenol) obtained from cashew industries as a byproduct is a unique amphiphilic molecule, which can be functionalized in many ways, producing an array of multifunctional molecules.[13−16] Several nanostructured functional materials were reported through hierarchical self-assembling of functionalized cardanol.[17−19] Here, we are demonstrating the development of quaternary ammonium salts derived from 3-pentadecylphenol by a two-step strategy involving Williamson type etherification, followed by Menschutkin quaternization.[20] They have a unique structure with a hydrophobic pentadecyl group as the tail and a quaternary ammonium salt as the ionic headgroup and are expected to form self-assembled hierarchical supramolecular architectures through a combination of noncovalent interactions. Subtle changes in the director of the self-assembled aggregates by the influence of temperature and solvent are expected to induce transformation into crystalline and liquid crystalline phases.

## RESULTS AND DISCUSSION

Quaternary ammonium salts of 3-pentadecylphenol, with spacer lengths of 2, 4, and 8, were prepared by following a two-step strategy of Williamson type etherification, followed by quaternization via the Menschutkin reaction (Scheme 1), and

Received: December 13, 2013
Accepted: February 26, 2014
Published: February 26, 2014

   dx.doi.org/10.1021/am4057453 | ACS Appl. Mater. Interfaces 2014, 6, 4126−4133

were designated as QS2, QS4, and QS8, and the experimental details are as reported in the Supporting Information.

**Scheme 1. Preparation of QS2, QS4, and QS8**

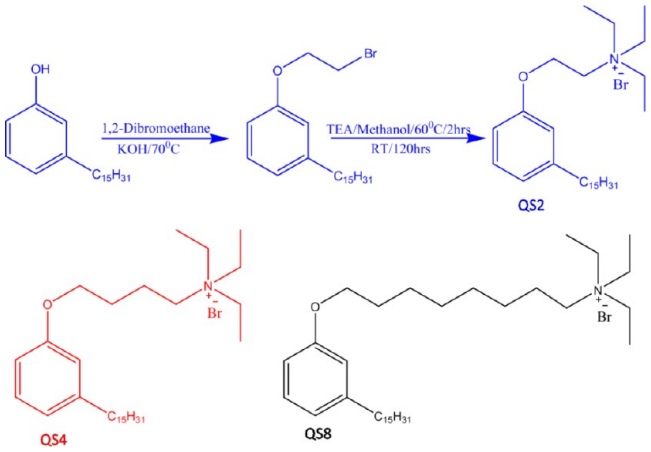


Formation of the targeted compounds was confirmed by elemental analysis, HRMS, FT-IR, $^{1}$HNMR, and $^{13}$CNMR, and the details are given in the Supporting Information (see Figures S1−S6). Concentration-dependent absorption and emission studies were carried out for determing the critical micelle concentration as shown in Figure S7 (see the Supporting Information).

**Morphology and Liquid Crystalline Phase Formation.** Investigation of the liquid crystalline phase formation of QSs is of great interest since the refractive index, electric permittivity, and the mechanical properties depend on the direction in which these quantities are measured. Liquid crystalline phase transitions of QS2, QS4, and QS8 were studied under temperature-induced (thermotropic) and solvent-induced (lyotropic) conditions. Thermotropic phase transitions were investigated using combined techniques of DSC and hot stage PLM, whereas lyotropic phase transitions were manifested from the observation of textural changes under PLM in combination with rheological property measurements. Generally, during heating, all QSs partially melted, losing their crystallinity, and exhibited a series of complex mesophases with characteristic textures and finally changed into an isotropic liquid.

DSC scans showing mesophase transitions during the first and second heating and cooling scans of QS2 are shown in Figure 1e. QS2 showed phase transition from crystalline to plastic crystalline at 28.59 °C ($\Delta H$ = 11.58 J/g). On further heating, the plastic crystalline phase changed into hexagonal columnar ($Co_h$) at 37.65 °C ($\Delta H$ = 44.37 J/g). QS2 melts at 113.82 °C completely. On cooling from the melt, it forms nematic droplets around 117.7 °C ($\Delta H$ = −0.87 J/g), which slowly transforms into the columnar phase around 60 °C ($\Delta H$ = −3.2 J/g). On further cooling, it changed into the plastic crystalline phase at 20.6 °C ($\Delta H$ = −12.56 J/g) and then to the crystalline phase at 4.85 °C ($\Delta H$ = −45.78 J/g). On second heating after holding at 0 °C for 5 min, QS2 showed an intense peak around 38.5 °C ($\Delta H$ = 73.78 J/g) corresponding to the transition from crystalline to columnar phase, that is, three-dimensional crystalline phase to two-dimensional columnar phase, and further it follows the same trend as in the initial scan.

On cooling, QS2 exhibited nematic droplets around 115.8 °C ($\Delta H$ = −0.58 J/g), which was further transformed into columnar at 89.8 °C ($\Delta H$ = −1.26 J/g). On further cooling, columns organized into the plastic crystalline phase around 35.8 °C ($\Delta H$ = −10.99 J/g) and then the crystalline phase around 8.42 °C ($\Delta H$ = −18.07 J/g). In both scans, a difference of ∼25−30 °C between the crystalline−mesophase transition and recrystallization during cooling was observed, revealing the existence of a supercooled state. However, phase transition studies in QS4 and QS8 could not observe any plastic crystalline phase. They exhibited columnar focal conic phases on heating and nematic and columnar mesophases on cooling and finally transform to the crystalline phase on supercooling. The details of thermotropic phase transitions of QSs on the second scan are summarized in Table 1. The representative columnar phases of QS2, QS4, and QS8 and the plastic crystalline phase of QS2 are given in panels a−d in Figure 1, respectively.

In the cooling cycle, the isotropic phase of QS8 changed homogeneously to nematic droplets with a birefringent shell around 117 °C (Figure 2a). On further cooling, we observed a series of dynamic structural orientations and deformations under PLM. The PLM image showing apparent enhancement in the birefringence of the nematic droplet is shown in Figure 2b. Later, the center of the nematic shell was observed to be

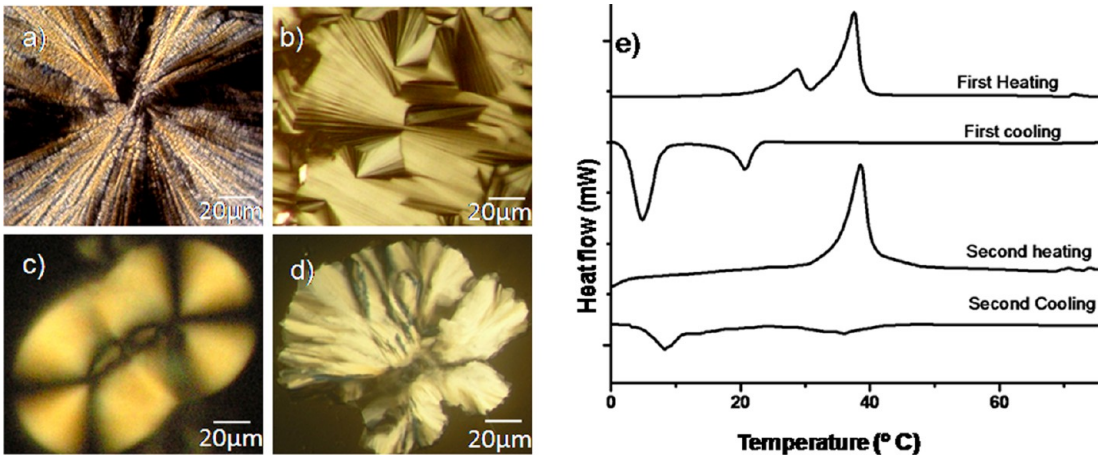


**Figure 1.** PLM images of columnar phases of QSs: (a) QS2, (b) QS4, and (c) QS8. (d) Plastic crystalline phase observed in QS2. (e) DSC scans of QS2 showing mesophase phase transitions on heating and cooling.


dx.doi.org/10.1021/am4057453 | ACS Appl. Mater. Interfaces 2014, 6, 4126−4133

**Table 1. Thermotropic Phase Transitions of QSs on Second Heating**

| QSn | transition | temperature (°C) | $\Delta H$ (J/g) |
|---|---|---|---|
| QS2 | Cr[a]–$Co_h$[b] | 38.5 | 73.78 |
| | $Co_h$–I[c] | 113.82 | 96.7 |
| QS4 | Cr–$Co_h$ | 36.77 | 50.4 |
| | $Co_h$–I | 112.84 | 97.5 |
| QS8 | Cr–$Co_h$ | 18.35 | 1.5 |
| | $Co_h$–I | 111.63 | 48.8 |

[a]Crystalline. [b]Hexagonal columnar. [c]Isotropic.

blooms with bright multiple colors (Figure 2c), and later, a sharp bright yellow tip at the center was observed, resembling a diamond-like structure (Figure 2d). On further cooling, the center crashed with a defect (Figure 2e) and four extinction brushes were observed around each defect point, revealing the formation of the characteristic focal conic columnar phase at ~60 °C (Figure 2f). On further cooling, the columnar mesophase reoriented to form the crystalline phase. DSC curves of QSs on the second scan and the characteristic crystalline phases of QSs are given in the Supporting Information (Figure S8).

Lyotropic phase transition studies of aqueous solutions of QSs were performed using PLM in combination with rheological analysis. Phase transitions were followed by performing rheological measurements and simultaneous observation of texture under PLM. At very low concentration, QSs exhibited the isotropic phase with a negligibly small value of storage modulus and loss modulus, and on increasing the concentration (~$10^{-2}$ M), QSs aggregated into the micellar phase, which was confirmed by UV–vis spectroscopic measurements. Critical micellar concentrations were evaluated as $1.02 \times 10^{-2}$ M (QS2), $8.3 \times 10^{-3}$ M (QS4), and $8.2 \times 10^{-3}$ M (QS8), respectively, as described above. As the concentration increased (~$5 \times 10^{-2}$ M), they exhibited nematic columnar droplets (Figure 3a). Later, with increasing concentration (~$8 \times 10^{-2}$ M), the nematic phase transforms into the hexagonal columnar phase. The images of the columnar phase of QS4 observed under PLM, SEM, and AFM are shown in Figure 3b,c,e, respectively. On further increasing the concentration of QSs (~$1 \times 10^{-1}$ M), the columnar phase underwent spontaneous self-organization to form a birefringent fibrillar gel network.

Fibrillar images observed for QS4 under PLM, SEM, AFM, and TEM are given in Figure 3b,d,g,i, respectively. Figure 3b shows the coexistence of a fibrillar network and the columnar phase, which suggests the formation of a fibrillar network through the impulsive aggregation of the columnar phase. The width of the fiber is measured as 8.3 nm from TEM imaging. Height profiles of AFM images also reveal that the aggregation takes place in the nanoscopic regime. Gel formation via the hierarchical self-assembly of molecules through the formation of vesicular architectures and spontaneous transformation to a fibrous network was reported by other researchers.[21,22]

Further lyotropic phase formation was confirmed by measuring viscoelastic properties of QSs using a modulated compact rheometer. Storage modulus showed significant variation with the increase in concentration of QSs.

Generally, below $10^{-3}$ M, QSs exhibited the isotropic phase with a storage modulus in the range of ~400 Pa. When the concentration is in between $5 \times 10^{-3}$ and $3 \times 10^{-2}$ M, QSs exhibited a storage modulus of (~$10^4$ Pa) due to the inclusion of nematic droplets in the isotropic phase. On further increasing the concentration, the columnar phase was observed with an enhancement in $G'$ ($2.4 \times 10^4$ Pa (QS2), $5.6 \times 10^4$ Pa (QS4), and $8.8 \times 10^4$ Pa (QS8). Above $7 \times 10^{-2}$ M, QSs form the gel phase with a sharp hike in $G'$ and $G''$ values. Rheograms of QS2, QS4, and QS8 showed frequency-independent storage and loss modulus profiles, which is characteristic of the gel phase. A typical rheogram showing changes in the storage

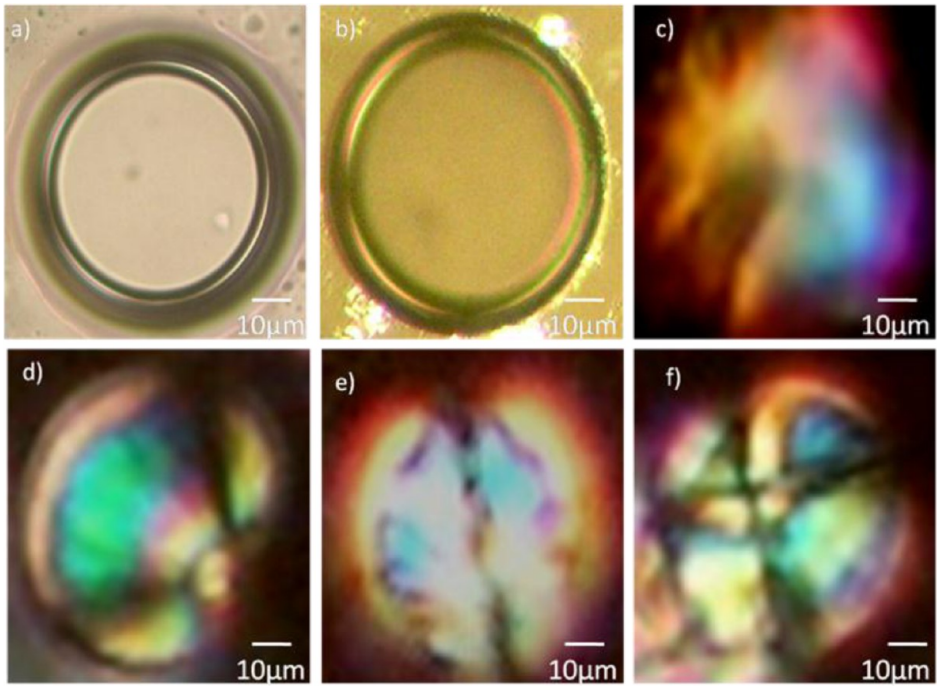


**Figure 2.** PLM images showing the sequence of mesophases that appeared during cooling from the isotropic melt of QS8: (a) nematic droplet at 117 °C, (b–e) various phase changes during cooling from 117 to 60 °C, (f) columnar phase formation at 60 °C.

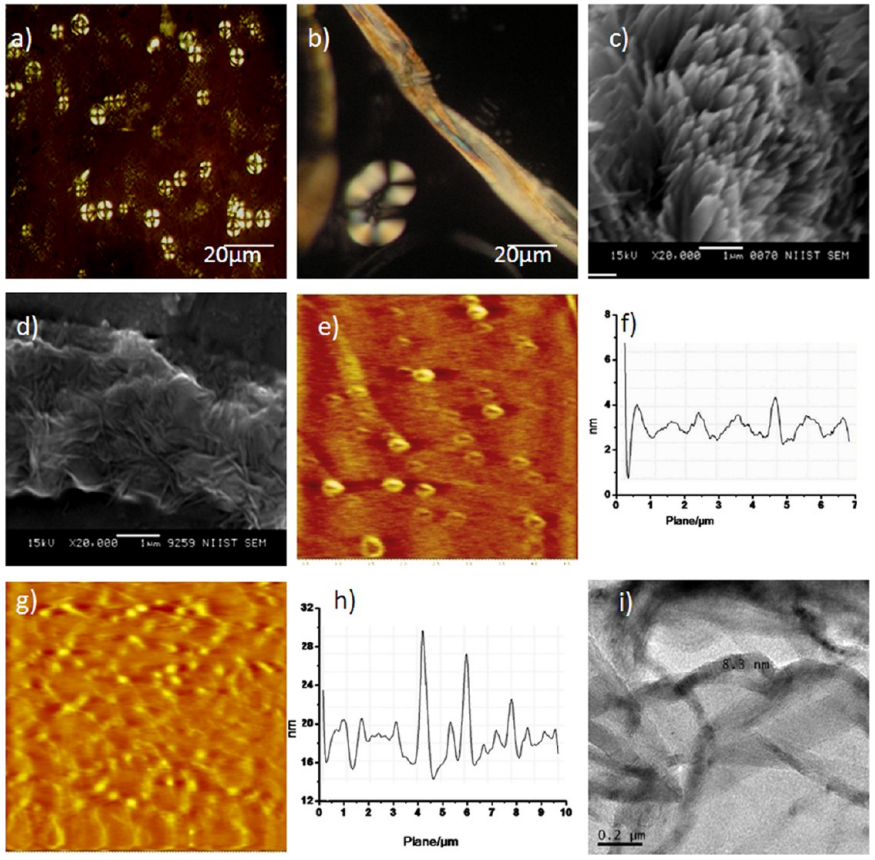


**Figure 3.** Microscopic images observed during lyotropic phase formation of QS4. Formation of columnar at $5 \times 10^{-2}$ M: (a) PLM, (c) SEM, (e) AFM. Aggregation of columnar mesophase to fibrils ($1 \times 10^{-1}$ M): (b) PLM, (d) SEM, (g) AFM, and (i) TEM. (f) and (h) Height profiles of AFM images.

modulus, loss modulus, and complex viscosity under an angular frequency sweep in the gel phase of QS8 is shown in Figure 4.

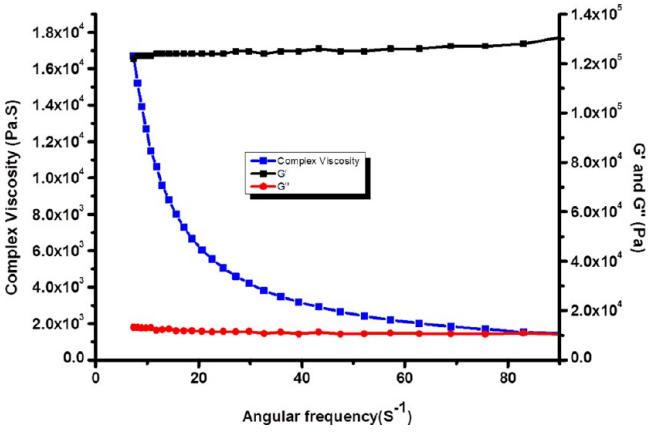


**Figure 4.** Rheogram taken at the gel phase (QS8) showing variation of storage modulus, loss modulus, and complex viscosity under an angular frequency sweep with an angular strain of 1%.

Complex viscosity decreased from $1.6 \times 10^4$ to $1.6 \times 10^3$ Pa S with increasing angular frequency. The concentration at the onset of the gel phase for QS2 and QS4 was observed to be $8 \times 10^{-2}$ and $7.5 \times 10^{-2}$ M, respectively. The phase diagram showing the isotropic phase, anisotropic inclusion in the isotropic phase, columnar phase, and gel phase of QSs with respect to concentration and storage modulus is shown in Figure 5. Normally, all the QSs exhibited an almost similar phase profile except for the onset concentrations and the storage moduli values. These deviations arise from the changes in the mode of packing attributed to the difference in the length of alkyl chains.

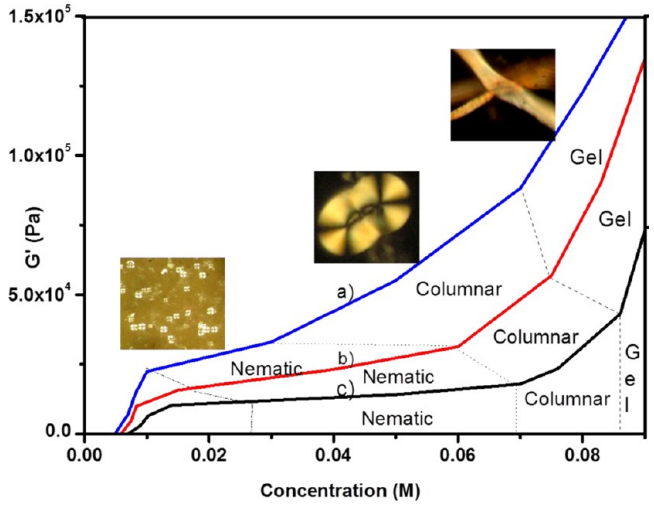


**Figure 5.** Phase diagram showing variation of storage modulus with respect to concentration: (a) QS8, (b) QS4, and (c) QS8. The PLM images showing the appearance of nematic, columnar, and gel phases in succession are shown in the insets.


dx.doi.org/10.1021/am4057453 | ACS Appl. Mater. Interfaces 2014, 6, 4126−4133

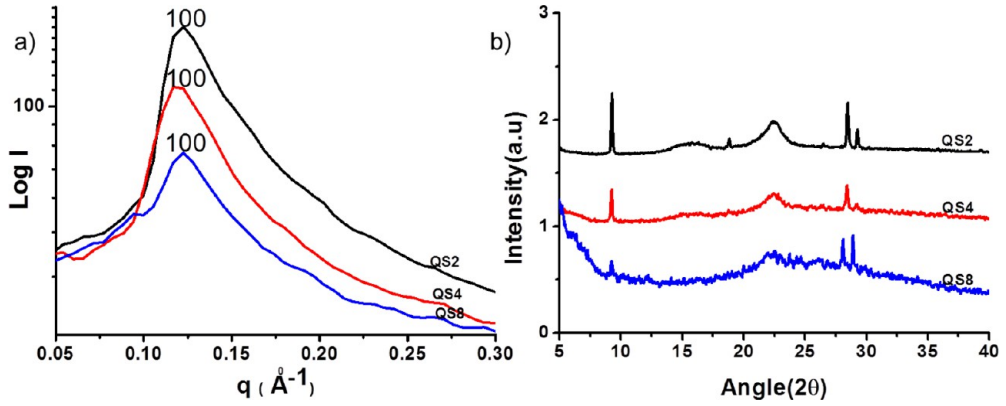


**Figure 6.** (a) SAXS patterns showing the signals corresponding to the (100) plane of hexagonal system. (b) Powder XRD patterns of QSs.

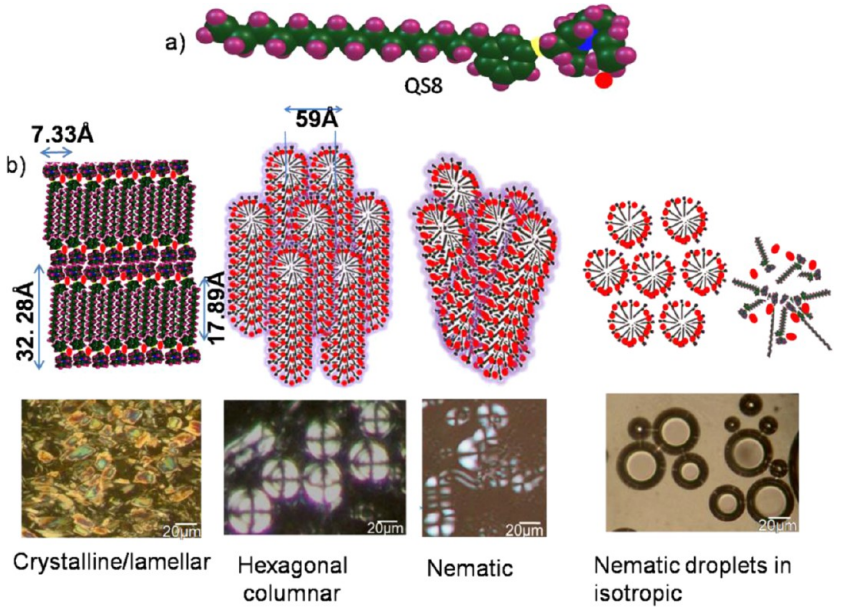


**Figure 7.** (a) Optimized geometry of QS8 using B3LYP method. (b) Schematic diagram showing isotropic phase, nematic droplets, nematic ribbon phase, hexagonal columnar and lamellar phases formed by self-organization through Coulombic forces, ion−dipole interactions, hydrophobic layer stacking, and interplanar $\pi-\pi$ stacking comprising ammonium ions, bromide ions, alkyl chains, and aromatic rings with their respective PLM images.

**XRD.** The crystalline nature and dimension of the ordered assemblies were studied using powder XRD combined with SAXS analysis. Generally, all QSs showed a sharp peak with a scattering vector value of $q = 0.122$ Å$^{-1}$, which is indexed as the (100) plane of the hexagonal lattice (Figure 6a).[23] The hexagonal lattice parameter is calculated using the equation

$$\alpha = \frac{4\pi}{\sqrt{3}q_a}$$

where $\alpha$ is the hexagonal lattice parameter and $q_a$ is the scattering vector corresponding to the 100 plane and was calculated as 59 Å. XRD powder patterns of QS2, QS4, and QS8 are shown in Figure 6b.

WAXD pattern of QSs exhibited a strong peak at $2\theta = 9.6°$ corresponding to a $d$-spacing of 9.2 Å. This $d$-spacing corresponds to the distance between the aromatic core stacking of QSs, which is found to be increased on moving from QS2 to QS8. They showed a broad halo around $2\theta = 22.64°$ with a $d$-spacing of 3.92 Å, which corresponds to the interlayer distance between the molecular chains. In addition, a relatively narrow sharp peak was observed at $2\theta = 28.64°$ with a $d$-spacing of 3.1 Å, which is the intracolumnar distance between the cores in the hexagonal lattice. Energy-minimized structures of bilayered QSs were obtained by the optimization studies using Gaussian with the B3LYP method using the 3-21g basis set (Figure S9 in the Supporting Information). The observed $d$-spacings almost agree with the various reflections measured from XRD. However, small discrepancies were observed arising from the influence of several noncovalent interactions among the molecular chains of QSs.

**Mechanism for LC Phase Formation.** The mechanism for the formation of various crystalline/plastic crystalline and liquid crystalline phases in QSs could be manifested from the studies made by PLM, DSC, rheology, and XRD. The schematic diagram showing the molecular layer ordering in different phases of QSs and the respective PLM pictures is shown in Figure 7. The energy-minimized structure of QS8 showed a bent-core geometry, as shown in Figure 7. It has been reported that molecules with a bent-core shape exhibited intriguing new features in comparison with LCs formed with rod- and disc-type molecules.[24] They can form self-assembled supramolecular architectures through various interactions, such as Coulombic

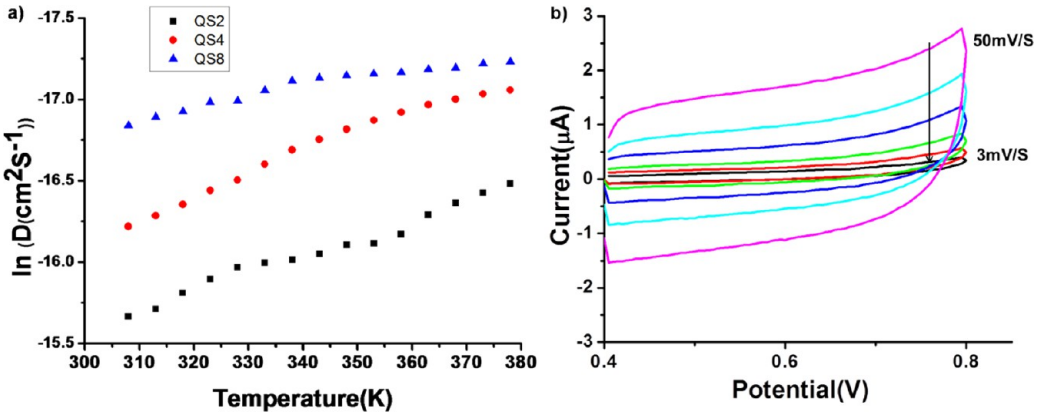


**Figure 8.** (a) Temperature-dependent variation of charge diffusion coefficients of QSs on cooling. (b) Electrochemical stability studies confirming stable electrochemical window of QS2 with varying scan rates (3−50 mV/S).

forces among the cations (ammonium) and anions (bromide) present in the ionic head groups, and can also form a interdigitated self-assembled structure via antiparallel stacking of the alkyl chains through electrostatic layer-by-layer assembling. The influence of anion type, alkyl chain length, and the location of the ionic charges on the liquid crystalline phase formation has been investigated earlier.[25] Accordingly, the nature of the mesophase formed depends on the surface alignment of self-assemblies, topographical defects, and molecular ordering, which are governed by various noncovalent interactions among the molecules, temperature, polarity, and quality of the solvent. Investigation of the LC phase formation of QSs under PLM reveals polymorphic textures, including crystalline, plastic crystalline, nematic, and hexagonal columnar phases. Molecular layers in the isotropic phase are randomly oriented, as shown in the Figure 7. In the nematic phase, molecular layers are uniaxially oriented and the plane of molecular layers may be perpendicular to the director.[26] However, columnar layers are biaxially oriented and the molecular layers in this phase are perpendicular to the layer planes. A slight tilt in the director angle is responsible for the observation of various textures arising from the difference in the nature of defects. Generally, at room temperature, QSs are three dimensionally ordered crystalline solids with highly birefringent spherulitic textures. During heating, they undergo a transition to the hexagonal columnar phase by losing their positional order. Further heating may possibly impart more kinetic energy to the molecules so that they unwind from the columns, resulting in less-ordered nematic phases. It could make the molecular layers in a disordered state of the isotropic phase with no features under PLM on further heating.

On cooling, individual mobile molecules loss their degree of freedom partially and associate together by means of electrostatic interactions between the ionic head regions and layer-by-layer interdigitation of alkyl chains to form nematic droplets, as shown in the cartoon (Figure 7). Further cooling results in the ordering of droplets in three dimension, which leads to the hexagonal columnar mesophase. Approaching of micellar droplets to close proximity is prevented by the repulsive interactions between the polar ends leaving nanochannels in between the columns. SAXS patterns of QSs exhibited the characteristic *d*-spacing of ∼59 Å, the intercolumnar distance of columns with a hexagonal symmetry. The observed *d*-spacing is longer than that calculated from Gaussian optimization for double chain length, confirming the existence of intercolumnar channels. Powder XRD patterns confirm that the phases are generated by the chain interdigitation of bent-core molecules (*d*-spacing ∼ 3.9 Å). On further cooling, QSs produce plastic crystalline/crystalline phases by the three-dimensional ordering of molecular chains. Another interesting observation we made is that only QS2 exhibited the plastic crystalline phase. The observed discrepancy in the LC phase formation among QS2 and QS4/QS8 can be explained on the basis of the alkyl chain length. With the increase in chain length, the quaternary center becomes less positive due to the electron releasing effect, and it results in weaker electrostatic interactions. Formation of multiple mesophases on cooling resulted from the frustration experienced by the spherical shell during the transition from nematic to columnar phases. Revannasiddaiah et al. made the same observation based on the optical sign of this uniaxial phase, which depends on the alkyl chain length.[27] These observations were further strengthened by the report made by Mermin.[28] Further, it was reported that LCs could exhibit different textures that depend upon the molecular shape, effect of surface alignment, and topological defect arising from the variations in the molecular organizations.[29,30]

**Ionic Conductivity.** Ionic conductivity exhibited by ILCs is receiving importance due to significant applications in electronic devices and drug delivery systems.[31] Conductivity depends both on the number of charge carriers and on their mobility. At room temperature, QSs exhibited a conductivity of $5 \times 10^{-4}$ S·cm$^{-1}$ (QS2), $2 \times 10^{-3}$ S·cm$^{-1}$ (QS4), and $8.2 \times 10^{-3}$ S·cm$^{-1}$ (QS8). The low conductivity values are due to the high extent of interaction between the ions in the crystalline state. As the temperature increased, the three-dimensional order present in the crystalline phase decreased and transforms into two/one dimensionally ordered LC phases where there is more freedom for the transport of charge carriers leading to higher conductivity. This conductivity enhancement with temperature is attributed to the thermotropic phase transitions that can be further envisaged from the temperature-dependent variation of charge diffusion coefficient ($D$) values.[32] It generally varies exponentially with temperature, and discontinuity in the profile is attributed to the phase transitions to produce conductive mesophases.[33] QSs exhibited multilinear variation of the diffusion coefficient with temperature on cooling corresponding to the thermotropic transitions from liquid crystalline to crystalline phases (Figure 8a). In QS8 and QS4, discontinuity was observed at ∼328 and ∼337 K, respectively, due to changes in the ordering of the molecular


dx.doi.org/10.1021/am4057453 | ACS Appl. Mater. Interfaces 2014, 6, 4126−4133

layers leading to mesophase transition. However, QS2 exhibited two discontinuities at ~353 and ~328 K corresponding to the liquid crystalline to plastic crystalline and plastic crystalline to crystalline transitions. This could highlight the presence of charge transport pathways as discontinuities in the liquid crystalline phases of QSs.

QSs exhibited ionic conductivities of $2.9 \times 10^{-3}$ S·cm$^{-1}$ (QS2), $11.2 \times 10^{-3}$ S·cm$^{-1}$ (QS4), and $16.7 \times 10^{-3}$ S·cm$^{-1}$ (QS8) at their columnar phase at 90 °C due to the increased mobility of charge carriers in the less-ordered phase. The effect of concentration of QSs in water on the ionic conductivity was measured. As the concentration varied from $7.5 \times 10^{-3}$ to $1 \times 10^{-1}$ M, the ionic conductivity values increased from $1.74 \times 10^{-3}$ to $22.34 \times 10^{-3}$ S·cm$^{-1}$ for QS8 at 70 °C. This suggests its application as an anisotropic conductor in high-energy devices.

Electrochemical properties of the QSs were studied by performing cyclic voltammetric analysis. An electrochemical cell was fabricated with a three-electrode system comprising a glassy carbon working electrode, a platinum counter electrode, and a standard calomel reference electrode using a 0.1 M solution of QS2 in acetonitrile as electrolyte. CV analysis showed a reasonably good electrochemical window that decreased with increasing spacer length. On moving from QS2 to QS8, the anodic stability decreased while the cathodic stability remains almost the same. The cationic center becomes less positive with the increase in electron releasing alkoxy chain length, which, in turn, reduces its oxidation potential. The observed reduction potentials are lower than those of common aliphatic quaternary salts due to the presence of an aromatic conjugated $\pi$-electron core, which reduces the cathodic stability.[8] Cyclic voltammograms of QSs are given in Figure S10 (Supporting Information). It showed good electrical stability on varying scan rates from 3 to 50 mV/S, which suggests its application as an electrolyte in electronic devices (Figure 8b).

## CONCLUSION

Ionic liquid crystals based on quaternary ammonium salts of 3-PDP were prepared successfully with high purity and yield by a simple facile strategy. Amphotropic liquid crystalline phase transition studies using various techniques revealed the formation of crystalline, plastic crystalline, nematic, and hexagonal columnar phases. On the basis of the microscopic, rheological, and XRD analysis, the phase diagram and mechanism for the observed LC and gel phases have been suggested. Temperature- and concentration-dependent ionic conductivity measurements revealed an anisotropic ionic conductivity of $\sim 1.67 \times 10^{-2}$ S/cm, which suggests their application in high-energy devices. Diffusion coefficient measurements confirm the existence of conductive pathways in the LC phase of QSs. Electrochemical stability studies showed a good electrochemical window for QS2, suggesting its application as a prospective electrolyte in supercapacitors. This is the first report on the preparation of conductive liquid crystalline/gel derived from the very low cost renewable resource material based on cardanol.

## ASSOCIATED CONTENT

### Supporting Information

Experimental procedures of reactions, UV–vis and FT-IR spectra, CMC determination, DSC thermograms, PLM of crystalline phases, optimized structures, FAB-mass spectra of QSs, and the details of instrumentation used for the characterizations. This material is available free of charge via the Internet at http://pubs.acs.org.

## AUTHOR INFORMATION

### Corresponding Author

*E-mail: sudhajd2001@yahoo.co.in.

### Author Contributions

All authors have given approval to the final version of the manuscript.

### Notes

The authors declare no competing financial interest.

## ACKNOWLEDGMENTS

We thank CSIR-UGC and CSIR network project Multifun CSC0101 and TAPSUN (NWP-54) for the financial support. We also thank Dr. Suresh Das, Director, NIIST, TVM, and Dr. A. Ajayaghosh, Dean AcSIR, NIIST, TVM, for their constant encouragement and support. We are also thankful to P. Gurusamy, Dr. E. Bhoje Gowd, M. Chandran, Lucy Paul, and Kiran Mohan for XRD, SEM, and TEM analyses.

## REFERENCES

(1) Brennecke, J. F.; Maginn, A. J. Ionic Liquids: Innovative Fluids for Chemical Processing. *AIChE J.* **2001**, *47*, 2384–2389.

(2) Lee, C. K.; Huang, H. W.; Lin, I. J. B. Simple Amphiphilic Liquid Crystalline *N*-Alkylimidazolium Salts. A New Solvent System Providing a Partially Ordered Environment. *Chem. Commun.* **2000**, 1911–1912.

(3) Shimura, H.; Yoshio, M.; Hoshino, K.; Mukai, T.; Ohno, H.; Kato, T. Noncovalent Approach to One-Dimensional Ion Conductors: Enhancement of Ionic Conductivities in Nanostructured Columnar Liquid Crystals. *J. Am. Chem. Soc.* **2008**, *130*, 1759–1765.

(4) Chen, X.; Tenneti, K. K.; Li, C. Y.; Bai, Y.; Zhou, R.; Wan, X.; Fan, X.; Zhou, Q. F. Design, Synthesis, and Characterization of Bent-Core Mesogen-Jacketed Liquid Crystalline Polymers. *Macromolecules* **2006**, *39*, 517–527.

(5) Binnemans, K. Ionic Liquid Crystals. *Chem. Rev.* **2005**, *105*, 4148–4204.

(6) Gordon, C. M.; Holbrey, J. D.; Kennedy, A. R.; Seddon, K. R. Ionic Liquid Crystals: Hexafluorophosphate Salts. *J. Mater. Chem.* **1998**, *8*, 2627–2636.

(7) Min, G. H.; Yim, T.; Lee, H. Y.; Huh, D. H.; Lee, E.; Mun, J.; Oh, S. M.; Kim, Y. G. Synthesis and Properties of Ionic Liquids: Imidazolium Tetrafluoroborates with Unsaturated Side Chains. *Bull. Korean Chem. Soc.* **2006**, *27*, 847–852.

(8) Sato, T.; Masuda, G.; Takagi, K. Electrochemical Properties of Novel Ionic Liquids for Electric Double Layer Capacitor Applications. *Electrochim. Acta* **2004**, *49*, 3603–3611.

(9) Hanyu, Y.; Honma, I. Rechargeable Quasi-Solid State Lithium Battery with Organic Crystalline Cathode. *Sci. Rep.* **2012**, *2*, No. 453.

(10) Ribot, J. C.; Sanchez, C. G.; Hoogenboom, R.; Schubert, U. S. Thermoreversible Ionogels with Tunable Properties via Aqueous Gelation of an Amphiphilic Quaternary Ammonium Oligoether-Based Ionic Liquid. *J. Mater. Chem.* **2010**, *20*, 8279–8284.

(11) Bandara, T. M. W. J.; Dissanayake, M. A. K. L.; Jayasundara, W. J. M. J. S. R.; Albinsson, I.; Mellander, B. E. Efficiency Enhancement in Dye Sensitized Solar Cells Using Gel Polymer Electrolytes Based on a Tetrahexylammonium Iodide and $MgI_2$ Binary Iodide System. *Phys. Chem. Chem. Phys.* **2012**, *14*, 8620–8627.

(12) Wei, Z.; Wei, X.; Wang, X.; Wang, Z.; Liu, J. Ionic Liquid Crystals of Quaternary Ammonium Salts with a 2-Hydroxypropoxy Insertion Group. *J. Mater. Chem.* **2011**, *21*, 6875–6882.

(13) Sudha, J. D.; Sasikala, T. S. Studies on the Formation of Self-Assembled Nano/Microstructured Polyaniline–Clay Nanocomposite (PANICN) Using 3-Pentadecyl Phenyl Phosphoric Acid (PDPPA) as a Novel Intercalating Agent Cum Dopant. *Polymer* **2007**, *48*, 338–347.

(14) Bhavsar, G. A.; Asha, S. K. Pentadecyl Phenol- and Cardanol-Functionalized Fluorescent, Room-Temperature Liquid-Crystalline Perylene Bisimides: Effect of Pendant Chain Unsaturation on Self-Assembly. *Chem.—Eur. J.* **2011**, *17*, 12646−12658.
(15) Sudha, J. D.; Reena, V. L. Structure Directing Effect of Renewable Resource Based Amphiphilic Dopants on the Formation of Conducting Polyaniline-Clay Nanocomposite. *Macromol. Symp.* **2007**, *254*, 274−283.
(16) Sudha, J. D.; Reena, V. L.; Pavithran, C. Facile Green Strategy for Micro/Nano Structured Conducting Polyaniline-Clay Nanocomposite via Template Polymerization Using Amphiphilic Dopant, 3-Pentadecyl Phenol 4-Sulphonic Acid. *J. Polym. Sci., Part B: Polym. Phys.* **2007**, *45*, 2664−2673.
(17) Ikkala, O.; Brinke, G. Hierarchical Self-Assembly in Polymeric Complexes: Towards Functional Materials. *Chem. Commun.* **2004**, 2131−2137.
(18) John, G.; Balachandran, V. S.; Jadhav, S. R.; Vemula, P. K. Recent Advances in Cardanol Chemistry in a Nutshell: From a Nut to Nanomaterials. *Chem. Soc. Rev.* **2013**, *42*, 427−438.
(19) Sudha, J. D.; Sivakala, S. Conducting Polystyrene/Polyaniline Blend through Template Assisted Emulsion Polymerisation. *Colloid Polym. Sci.* **2009**, *287*, 1347−1354.
(20) Stanger, K. J.; Lee, J. J.; Smith, B. D. Dramatic Acceleration of the Menschutkin Reaction and Distortion of Halide Leaving-Group Order. *J. Org. Chem.* **2007**, *72*, 9663−9668.
(21) Kartha, K. K.; Mukhopadhyay, R. D.; Ajayaghosh, A. Supramolecular Gels and Functional Materials Research in India. *Chimia* **2013**, *67*, 51−63.
(22) Hirai, Y.; Babu, S. S.; Praveen, V. K.; Yasuda, T.; Ajayaghosh, A.; Kato, T. Anisotropic Self-Assembly of Photoluminescent Oligo (*p*-Phenylene Vinylene) Derivatives in Liquid Crystals: An Effective Strategy for the Macroscopic Alignment of Gels. *Adv. Mater.* **2009**, *21*, 4029−4033.
(23) Wang, Z.; Liu, F.; Gao, Y.; Zhuang, W.; Xu, L.; Han, B.; Li, G.; Zhang, G. Hexagonal Liquid Crystalline Phases Formed in Ternary Systems of Brij 97−Water−Ionic Liquids. *Langmuir* **2005**, *21*, 4931−4937.
(24) Seo, J.; Kim, S.; Gihm, S. H.; Park, C. R.; Park, S. R. Highly Fluorescent Columnar Liquid Crystals with Elliptical Molecular Shape: Oblique Molecular Stacking and Excited-State Intramolecular Proton-Transfer Fluorescence. *J. Mater. Chem.* **2007**, *17*, 5052−5057.
(25) Reddy, R. A.; Tschierske, C. Bent-Core Liquid Crystals: Polar Order, Superstructural Chirality and Spontaneous Desymmetrisation in Soft Matter Systems. *J. Mater. Chem.* **2006**, *16*, 907−961.
(26) Liang, H. L.; Schymura, S.; Rudquist, P.; Lagerwall, J. Nematic-Smectic Transition under Confinement in Liquid Crystalline Colloidal Shells. *Phys. Rev. Lett.* **2011**, *106*, 247801.
(27) Revannasiddaiah, N. D.; Krishnamurti, D. Optical Behaviour of Mixtures of Nematic and Cholesteric Compounds. *Mol. Cryst. Liq. Cryst.* **1983**, *101*, 103−127.
(28) Mermin, N. D. The Topological Theory of Defects in Ordered Media. *Rev. Mod. Phys.* **1979**, *51*, 591−648.
(29) Senyuk, B.; Wonderly, H.; Mathews, M.; Li, Q.; Shiyanovskii, S. V.; Lavrentovich, O. D. Surface Alignment, Anchoring Transitions, Optical Properties, and Topological Defects in the Nematic Phase of Thermotropic Bent-Core Liquid Crystal A131. *Phys. Rev. E* **2010**, *82*, 041711.
(30) Lopez-Leon, T.; Nieves, A. F.; Nobili, M.; Blanc, C. Nematic-Smectic Transition in Spherical Shells. *Phys. Rev. Lett.* **2011**, *106*, 247802−247805.
(31) Noujeim, N.; Samsam, S.; Eberlin, L.; Sanon, S. H.; Rochefort, D.; Schmitzer, A. R. Mesomorphic and Ion Conducting Properties of Dialkyl(1,4-phenylene)diimidazolium Salts. *Soft Matter* **2012**, *8*, 10914−10920.
(32) Chidsey, C. E.; Feldman, B. J.; Lundgren, C.; Murray, R. W. Micrometer-Spaced Platinum Interdigitated Array Electrode: Fabrication, Theory, and Initial Use. *Anal. Chem.* **1986**, *58*, 601−607.
(33) Abate, A.; Petrozza, A.; Cavallo, G.; Lanzani, G.; Matteucci, F.; Bruce, D. W.; Houbenov, N.; Metrangolo, P.; Resnati, G. Anisotropic Ionic Conductivity in Fluorinated Ionic Liquid Crystals Suitable for Optoelectronic Applications. *J. Mater. Chem. A* **2013**, *1*, 6572−6578.